C-Band Digital Aeronautical Communication for Unmanned Aircraft Systems

Daniel M. Mielke*, *German Aerospace Center (DLR)*
*daniel.mielke@dlr.de

***Abstract*—The drone market is anticipated to make up of 10% of the European Union aviation market in the next ten years. Typical fields of operation are logistics/transportation, agriculture or surveillance tasks. Both Unmanned Aircraft (UAs) and traditional manned aircraft are sharing the same airspace. Therefore concepts for the integration of UAs into the controlled and uncontrolled airspace are mandatory. An essential part of this integration is the communication between all participants. Hence the development of reliable data links as well as channel models for different flight scenarios to validate the link concepts is required. In this paper we discuss the application of OFDM- and SC-FDMA-based communication links and test them against three flight scenarios: en-route, take-off and landing, and airport using Monte-Carlo simulations. We suggest different coding schemes and show that iterative decoding processes have disadvantages in case of insufficient channel estimation.**

I. Introduction

MORE and more UAs are expected to enter the skies both in the controlled and uncontrolled airspace during the next years. For example, the market for UAs in the European Union is expected to make up to $10\,\%$ of the European aviation market [1] during the next ten years. The anticipated fields of application are transportation or other logistic tasks, as well as surveillance, exploration, and tasks in the agronomy [2].

It is ruled out, that these UAs will operate completely autonomously and non-cooperatively. Hence, there is a need for a reliable communication system between the UAs and a central controlling instance and a remote pilot.

In the field of manned aviation, most communication is still performed using analogue voice radio [3]. However, more modern technologies have been applied to the aviation community during the last years, e. g. Aircraft Communications Addressing and Reporting System (ACARS) or Very High Frequency Data Link (VDL). While these systems are designed as an addition to the still indispensable analogue voice radio, new developments are on their way to provide a more modern communication system. The terrestrial solution is the L-Band Digital Aeronautical Communication System (LDACS) [4], [5]. It provides both voice communication and the exchange of additional information like flight tracks and telemetric data. Nonetheless, it has not been designed to fulfill the requirements for a Control and Non Payload Communications (CNPC) link for UAs as identified in [6], [7].

An adapted version of Long Term Evolution (LTE) is already used to provide Internet access to the passengers aboard of an airplane [8]. However, it is important to note that LTE is only used for payload communication, i. e. no CNPC data is transmitted over this link. Since LTE has not been designed for aviation purposes, it is not expected to fulfill the high-performance requirements for CNPC without adaptions. Aeronautical Mobile Airport Communication System (AeroMACS) is intended to become the standard for airport communication, operating from $5091\,\mathrm{MHz}$ to $5150\,\mathrm{MHz}$, [9]. However, its focus is on the air traffic management at airports and their environment [10].

Nonetheless, none of the systems above can supply a CNPC link as required for the safe operation of UAs. In this paper we propose a new system operating in the aeronautical C-band called C-Band Digital Aeronautical Communication System (CDACS) tailored to match all requirements defined in [6], [7]. The most relevant requirements according to these studies are low latency (maximum round trip latency of $2\,\mathrm{s}$ for $95\,\%$ of messages), high availability, and high continuity (joined overall delivery overall probability of up to $99.999\,\%$).

The suggested frequency range for such a system is between $5030\,\mathrm{MHz}$ and $5091\,\mathrm{MHz}$, a range that is only used by the very rare Microwave Landing System (MLS). Studies have shown that a coexistence is even possible in case the distribution of MLS grows [11]. Additionally, the impairments due to rain [12] and atmospheric gases [13] in C-band are acceptable. In this paper we propose the usage of different modulation concepts and coding schemes and discuss the results of Monte-Carlo simulations applied to our concepts.

It is structured as follows: After some discussion of the theory behind our channel models in Section II, we introduce our link design in Section III. We present some simulation results and discuss them in Sections IV and V, respectively.

II. Methods

An essential part one has to consider when designing a new communication system is the knowledge of the channel the data is transmitted through. Hence, it is common practice to develop channel models that simulate the behavior of the targeted channel. In the following we explain the channel models we have implemented for our simulations.

Multiple scenarios representing different phases of a typical flight of a manned aircraft have been identified [14]. We assume that this distinction holds for UAs as well. Additionally, we assume that all scenarios fulfill the conditions of the popular Wide Sense Stationary Uncorrelated Scattering (WSSUS) model [15].

The models are implemented as a discrete tapped delay line as illustrated in Fig. 1. Its impulse response at time t is given

TABLE I: Parameters of all channel models examined. $\mathcal{N}(\mu, \sigma^2)$ denotes a normal distribution with mean μ and variance σ^2, $\mathcal{U}(A)$ denotes a uniform distribution on interval A.

		ENR	TMA	APT
logarithmic K-factor	K_{dB}	$\mathcal{N}(29.4, 3.9)$	12	$\{8.9, 11, 12.5\}$
max. Doppler frequency	$f_{\mathrm{D,max}}$ [kHz]	5	1.32	0.14
RMS delay spread	σ_τ [µs]	0.01	1.05	1
Doppler spread	σ_{DS} [Hz]	-	$\mathcal{U}([20, 100))$	$\mathcal{U}([5, 60))$
Coherence Bandwidth	B_{c} [kHz]	2.000	78	117
Number of Taps	N_{tap}	up to 9	7	12

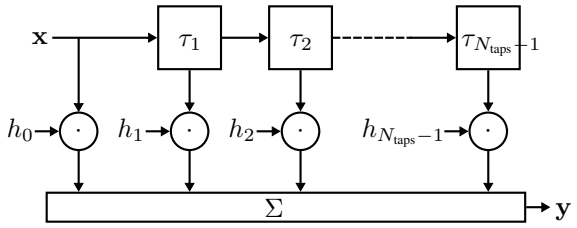

Fig. 1: Illustration of a tapped delay line model with N_{tap} taps. In general, all parameters are assumed to be time dependent. $\mathbf{x}$ is the input vector, $\mathbf{y}$ denotes the output vector.

by

$$h(t, \tau) = \sum_{i=0}^{N_{\mathrm{tap}}-1} h_i(t)\delta(\tau - \tau_i(t)), \tag{1}$$

where τ denotes the relative time, N_{tap} denotes the number of taps and $h_i(t)$ and $\tau_i(t)$ denote the i-th tap's (complex) weight and delay, respectively. The path weight $h_i(t)$ is defined as

$$h_i(t) = \alpha_i(t) e^{j \overbrace{[2\pi f_{\mathrm{D},i}(t) t + \varphi_i(t)]}^{\phi_i(t)}}, \tag{2}$$

with a Doppler frequency $f_{\mathrm{D},i}(t)$ and a phase $\varphi_i(t)$ that is assumed to be uniformly distributed on the interval of $[0, 2\pi)$. Tap $i = 0$ is defined as the Line of Sight (LOS) component and we set $\tau_0(t) = 0$ if not denoted otherwise. Finding reasonable values for $h_i(t)$ and $\tau_i(t)$ for the different scenarios is the key challenge in channel modeling when using the tapped delay line approach. Please note that we generally assume time varying parameters in our notation. In a time discrete environment, the time scale t translates to $t = kT_{\mathrm{SA}}$, with time index k and sample duration T_{SA}. If T_{SA} is chosen too large, this quantization can lead to an insufficient resolution of the path delays.

In the following, all scenarios are described in detail; Table I provides a condensed overview of all model parameters.

A. En-route Scenario - ENR

In the first scenario, the UA is at (or close to) its cruising speed and altitude. Measurement campaigns [16], [17] have shown that this scenario is dominated by a strong LOS path, completed by a ground reflected path and some comparatively weak multi path components.

A simple *Flat Earth Two Ray Model* is assumed for the first two taps:

$$\begin{aligned} h'_0(t) &= \frac{c_0}{4\pi d_{\mathrm{LOS}}(t) f_c} e^{j2\pi d_{\mathrm{LOS}}(t) f_c / c_0}, \; h_0(t) = \frac{h'_0(t)}{|h'_0(t)|} \\ h'_1(t) &= \frac{c_0}{4\pi d_{\mathrm{REF}}(t) f_c} e^{j2\pi d_{\mathrm{REF}}(t) f_c / c_0}, \; h_1(t) = \frac{h'_1(t)}{|h'_0(t)|} \\ \tau_1(t) &= (d_{\mathrm{REF}}(t) - d_{\mathrm{LOS}}(t))/c_0 \end{aligned} \tag{3}$$

where $d_{\{\mathrm{LOS,REF}\}}(t)$ denotes the link distance of the LOS path and the ground reflected path, respectively, assuming a carrier frequency f_c of 5 GHz.

The remaining parameters for $1 < i < N_{\mathrm{tap}}$ are randomly chosen, based on the results presented in [17]: First of all, it has been observed, that the additional taps are not always present, hence with a probability of $1 - P_{\mathrm{on},i}$ it is $h_i(t) = 0$. In the opposite case, the amplitude $\alpha_i(t)$ of each multi path component is computed from its power in dB generated by $\mathcal{N}(-26.1, 3.9)$. The tap delays $\tau_i(t)$ are set to the values suggested in [17].

Since the UA is around its top speed (assuming $v_{\mathrm{max}} \approx 300\,\mathrm{m\,s^{-1}}$), the maximum Doppler shift of $f_{\mathrm{D,max}} \approx 5\,\mathrm{kHz}$ is the highest of all scenarios. Due to the weak amplitudes of the multi path components and their low occurrence we assume the Doppler spread to be negligible.

B. Take-off and Landing - TMA

In the second scenario, the UA is either approaching or leaving the airport, i. e. it is clearly below cruising altitude; this scenario does also cover the acceleration/deceleration process on the runway. Our model is based on the AeroMACS measurement campaign results presented in [18] and the theoretical aspects discussed in [19]. The velocity of the UA is assumed to be significantly lower than during the ENR scenario, which reduces the impairments due to the Doppler effect; the maximum speed is assumed not to exceed $80\,\mathrm{m\,s^{-1}}$, hence the maximum Doppler frequency is set to $f_{\mathrm{D,max}} \approx 1.32\,\mathrm{GHz}$. The Doppler frequencies of the multi path components follow a Gaussian distribution with variances uniformly distributed between 20 Hz and 100 Hz and means uniformly distributed between $\pm f_{\mathrm{D,max}}$. The normalized Doppler power spectral density of an example instance of this channel model is plotted in Fig. 2a. The Doppler shift of the LOS component is clearly visible as well as the Doppler spread of the scattered components.

The delays of the multi path components are given by [15, (17)] as

$$\tau_i(t) = -\tau_{\text{slope}} \ln\{1 - u_i(1 - e^{-\tau_{\max}/\tau_{\text{slope}}})\}, \tag{4}$$

where $\tau_{\text{slope}} = 1\,\mu\text{s}$, $\tau_{\max} = 10\,\mu\text{s}$ and u_i is uniformly distributed on $[0, 1)$. The Power Delay Profile (PDP) is assumed to be exponentially decreasing and is given by

$$P_i(t) = \begin{cases} \frac{1}{1-e^{-\tau_{\max}/\tau_{\text{slope}}}} e^{-\tau_i(t)/\tau_{\text{slope}}}, & \text{if } 0 < \tau_i(t) \leq \tau_{\max} \\ 0, & \text{else.} \end{cases} \tag{5}$$

These powers are scaled such that the model achieves an average K-factor of around $K_{\text{dB}} \approx 12\,\text{dB}$ and converted to the multi path components' amplitudes.

C. Airport - APT

In the third scenario, the UA is either taxiing or parking; a LOS path or at least a comparatively strong reflected path is present. The presence of this specific path leads to Rician Fading. Its K-factor is selected from a set corresponding to different airports as presented in [20]. We assume a distribution of $P(K_{\text{dB}} = 8.9\,\text{dB}) = 0.2$, $P(K_{\text{dB}} = 11\,\text{dB}) = 0.5$ and $P(K_{\text{dB}} = 12.5\,\text{dB}) = 0.3$.

Due to its low speed, the maximum Doppler shift and the normal distributed Doppler frequencies of the multi path components are very low: $f_{\text{D,max}} = 140\,\text{Hz}$ and $\sigma_{\text{DS}} \sim \mathcal{U}([5\,\text{Hz}, 60\,\text{Hz}))$. An example Doppler power spectral density is plotted in Fig. 2b. However, airport buildings and other scatterers cause a classical multi path environment. The channel model bases on the conclusions presented in [21]. According to these results, there are two sets of multi path components that can be distinguished, additionally to the LOS path:

- Up to eight paths with a delay uniformly distributed between $0.1\,\mu\text{s}$ and $1.2\,\mu\text{s}$
- Three paths with a delay uniformly distributed between $1.3\,\mu\text{s}$ and $3\,\mu\text{s}$.

The logarithmic PDP is given by

$$P_{i,\text{dB}}(t) = \begin{cases} -11\,\text{MHz} \cdot \tau_i(t) - 11, & \text{if } 0.1\,\mu\text{s} \leq \tau_i(t) < 1.1\,\mu\text{s} \\ -8\,\text{MHz} \cdot \tau_i(t) - 17, & \text{if } 1.1\,\mu\text{s} \leq \tau_i(t) < 1.8\,\mu\text{s} \\ -14.5\,\text{MHz} \cdot \tau_i(t) + 4, & \text{if } 1.8\,\mu\text{s} \leq \tau_i(t) < 2.8\,\mu\text{s} \\ -24\,\text{MHz} \cdot \tau_i(t) + 40, & \text{if } 2.8\,\mu\text{s} \leq \tau_i(t) < 3\,\mu\text{s} \end{cases} \tag{6}$$

and illustrated in Fig. 3.

III. Link Design

A. Channel Coding

Forward error correction codes are used for error protection. We consider two different coding schemes: A Reed-Solomon code concatenated with a convolutional encoder as used in LDACS [22], see Fig. 4a, and a turbo encoder, see Fig. 4b. Interleavers are used in both cases to mitigate the effect of burst errors.

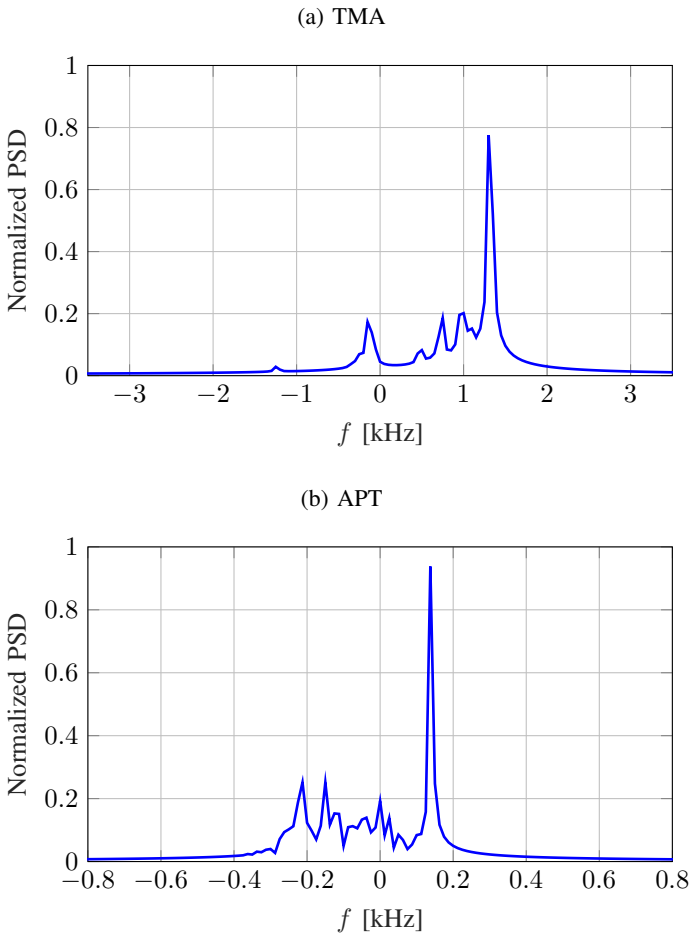

Fig. 2: These figures show the example Doppler Power Spectral Density (PSD) for the TMA and APT channel model. One can clearly observe the Doppler shift of the LOS component.

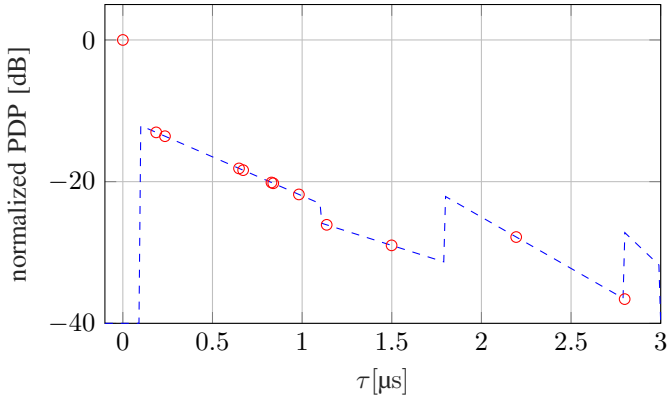

Fig. 3: Power Delay Profile (PDP) for the APT channel. The dashed line represents the general PDP mapping as given in Section II-C, the circles define example values. The item at $\tau = 0$ represents the LOS path.

The Reed-Solomon code for the outer coding is generated on the finite field (also known as Galois field) GF(8). Its primitive polynomial is given by

$$P(X) = X^8 + X^4 + X^3 + X^2 + 1. \quad (7)$$

The input bits $\mathbf{u}$ are encoded in blocks of size k_{blk}, resulting in blocks of size n_{interm}; the code rate is given by $R_{\text{RS}} \approx 0.9$. Each of these intermediate blocks is block interleaved and sent to a rate $R_{\text{CC}} \approx 0.5$ zero-terminated convolutional code defined by the generator polynomials $(171, 133)_{\text{OCT}}$ having a constraint length of $L = 7$. The encoding process is finalized by helix interleaving the n code bits. This coding scheme's overall code rate is $R_{\text{RSCC}} \approx 0.45$. On the receiver side, the Viterbi Algorithm using soft inputs is used for the decoding of the convolutional encoded bits.

The second forward error correction scheme implemented is a turbo encoder, as this class of codes is known to achieve a performance close to the Shannon limit in case of Additive White Gaussian Noise (AWGN). The turbo code used here consists of two parallel concatenated convolutional codes, defined by the generator polynomial $(23, 33)_{\text{OCT}}$ with a constraint length of $L = 5$ and a feedback connection given by $(23)_{\text{OCT}}$, [23]. The mother code has a rate of $R_{\text{TC}} \approx 0.33$, however, higher coding rates $R_{\text{TC,punct}}$ are achieved by puncturing. The decoding process is performed iteratively and terminated after N_{it} iterations.

B. Modulation

Unless denoted otherwise, we assume the code bits $\mathbf{c}$ to be mapped into Quadrature Phase Shift Keying (QPSK) symbols $\mathbf{s}$ using Gray mapping.

This symbol vector is further processed by either an Orthogonal Frequency Division Multiplex (OFDM) or Single Carrier Frequency Division Multiple Access (SC-FDMA) processing block.

OFDM is a popular concept used in lots of nowadays standards e. g. WiFi, LTE and others. It has also been proposed for aviation purposes, e. g. for AeroMACS and LDACS as it provides a high grade of flexibility. Another advantage is frequency diversity since it is a multi-carrier approach using N_{FFT} subcarriers.

A cyclic prefix of length $T_{\text{CP}} = T_{\text{SA}} N_{\text{CP}}$ is added before each OFDM symbol. If $T_{\text{CP}} > \max_{\forall i, \forall t}\{\tau_i(t)\}$ and perfect time synchronization is assumed, no inter symbol interference occurs at the cost of a reduced bandwidth efficiency and reduced signal to noise ratio.

Another key parameter for an OFDM system is the subcarrier spacing Δf, which is the inverse of the OFDM symbol duration T_S. If the upper bound of $\Delta f < \zeta B_c$, where B_c denotes the coherence bandwidth, is fulfilled, a single-tap equalizer is sufficient for equalization. ζ is a factor usually chosen between $[0.1, 0]$. The lower bound is given by the Doppler spread: $\Delta f > \sigma_{\text{DS}}$. Based on these restrictions, the OFDM parameters have been chosen as given in Table II.

OFDM's main drawback is the comparatively high Peak to Average Power Ratio (PAPR), an effect that becomes even more intense for an increasing number of subcarriers. A high PAPR leads to higher demands for the transmitter hardware [24].

TABLE II: Parameters for the implemented OFDM system

		OFDM
FFT length	N_{FFT}	64
Guard carriers	$N_{\text{G,l}}$ / $N_{\text{G,u}}$	7 / 6
Subcarrier spacing	Δf [kHz]	15
Overall bandwidth	B_{OFDM} [kHz]	960
Effective bandwidth	$B_{\text{OFDM,eff.}}$ [kHz]	750
OFDM symbol duration	T_{S} [µs]	66.66
Cyclic prefix	T_{CP} [µs]	11.45

SC-FDMA can be described as an Discrete Fourier Transform (DFT)-precoded OFDM system [25]. The symbols $\mathbf{s}$ are preprocessed by an M-point DFT before getting modulated by the N_{FFT}-Inverse Fast Fourier Transform (IFFT) with $M \leq N_{\text{FFT}}$. Consequently, only M out of the N_{FFT} subcarriers are used. The remaining subcarriers can be allocated to other users. This multi user property and the lower PAPR of the output signal (compared to OFDM) lead to our decision to propose SC-FDMA for the reverse link. However, in this paper we assume a single user to allocate all available subcarriers and did not consider multi user issues any further.

C. Channel Estimation and Equalization

Unless no perfect channel knowledge is assumed, the channel is estimated as follows.

For the OFDM case, pilot symbols are distributed over each frame in frequency domain. They are equally spaced with a distance of $N_{\text{plt},t} = 5$ in time and a distance of $N_{\text{plt},f} = 4$ in frequency direction.

For the SC-FDMA case, Zhadoff-Chu-sequences as applied in the LTE standard are used as pilot symbols. While the sequence is spread over all carriers, i. e. $N_{\text{plt},f} = 1$, the distance in time is $N_{\text{plt},t} = 5$.

The channel is estimated at the positions of the pilot symbols in frequency domain by dividing the received pilot symbol by the expected pilot symbol. A linear interpolation is used to estimate the remaining pilot symbols of the frame.

The equalization is performed following the zero-forcing approach by dividing each symbol of the received frame by the corresponding channel estimate.

The most important parts of the transmitter's and receiver's processing structure are illustrated in Fig. 5.

IV. Results

Several bit error curves versus the corresponding E_b/E_0 are plotted in Figs. 7 and 8 for the OFDM approach. Perfect channel knowledge is assumed for the plots in Fig. 7, while a pilot symbol based channel estimation with linear interpolation has been performed for the plots in Fig. 8, called *linear channel estimation* hereafter. Simulations have been run for all three channel models using the encoders as introduced above: a concatenated Reed-Solomon and convolutional code (RSCC) with an overall rate of $R_{\text{RSCC}} \approx 0.45$, a $R_{\text{TC}} \approx 0.33$ turbo code, and a punctured version of the same code with

(a) Reed-Solomon (RS) and convolutional encoder

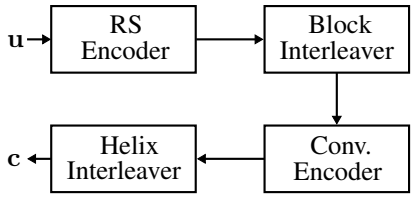

(b) Turbo Encoder: $\mathrm{ENC}_{\{0,1\}}$ denote convolutional encoders, P/S denotes a parallel-to-serial converter

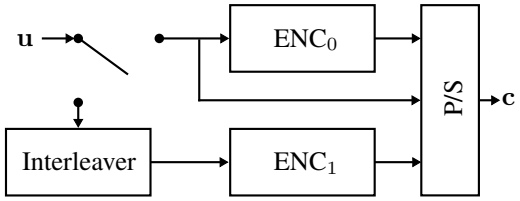

Fig. 4: Block diagrams of coding schemes: The information bits $\mathbf{u}$ get encoded into code bits $\mathbf{c}$.

$R_{\mathrm{TC,punct}} \approx 0.5$. A maximum a-posteriori based algorithm is used for the iterative decoding process, that is terminated after $N_{\mathrm{it}} = 6$ rounds.

For all channels and coding schemes, the system performs better if perfect channel knowledge is assumed. In this case, the RSCC code gets outperformed by the turbo codes for low values of E_b/E_0. However, the turbo codes show an error floor behavior for the TMA channel and are not capable of reaching a better BER than approximately 6×10^{-5}. They are both succumbing the RSCC code starting from an E_b/E_0 of $5\,\mathrm{dB}$. The curves of the APT scenario in Fig. 7c show a poor performance of the turbo codes; the RSCC code outperforms both of them, although its BER curve is much worse than for the other scenarios, especially for higher values of E_b/E_0.

The RSCC code is superior for all scenarios if linear channel estimation is applied. The turbo codes show the error floor effect for both the TMA and the APT scenario, see Figs. 8b and 8c. In case of the the APT channel, all coding schemes show a poor performance.

In Fig. 6, the BER curves for an SC-FDMA transmission over the TMA channel is plotted for both perfect channel knowledge and linear channel estimation. Again, the first is superior to the latter for all coding schemes. In case of perfect channel knowledge, the turbo codes outperform the RSCC approach. However, the error floor can be identified again. The overall performance is a little worse compared to OFDM, see Fig. 7b. Comparing Figs. 6a and 8b shows, that the RSCC code performs worse for the SC-FDMA approach, the performance of the turbo codes is slightly better.

V. Discussion

The results show that both OFDM and SC-FDMA are generally possible approaches for a communication system in the aeronautical C-band.

However, the channel scenarios used in this paper present diverse challenges to the communication system. While the performance of the applied coding is acceptable for the ENR scenario, all schemes basically fail for the APT scenario.

Comparing the results for perfect channel knowledge and the linear channel estimation illustrates the importance of a reliable channel estimation.

VI. Conclusion and Outlook

We have presented a set of channel models representing different phases of flight. The models have been designed using the results of different measurement campaigns for C-band. We have used these models to evaluate our proposed data links. The outcome of these tests is that OFDM and SC-FDMA are promising approaches to realize an aeronautical data link. However, the performance of the links must be further improved.

The planned future work on CDACS is to vary the parameters of the OFDM/SC-FDMA modulation, for example the amount of subcarriers, as well as coding parameters, e. g. the block size. Furthermore, the effect of different symbol alphabets like QAM with cardinalities of $M \in \{16, 64\}$ will be observed. Additionally, we expect a better performance in case of a more sophisticated channel estimation method, e. g. a Wiener filter based approach.

Acknowledgment

We would like to thank Pragadeeshwaran Pandianrajan for his support.

References

[1] "Ip/14/384: European commission calls for tough standards to regulate civil drones," 2014. [Online]. Available: http://europa.eu/rapid/press-release_IP-14-384_en.htm

[2] K. P. Valavanis and G. J. Vachtsevanos, *Handbook of Unmanned Aerial Vehicles*. Springer Publishing Company, Incorporated, 2014.

[3] D. Stacey, *Aeronautical Radio Communication Systems and Networks*. John Wiley & Sons Ltd, 2008.

[4] M. Schnell, U. Epple, D. Shutin, and N. Schneckenburger, "Ldacs: future aeronautical communications for air-traffic management," *IEEE Communications Magazine*, vol. 52, no. 5, pp. 104–110, May 2014.

[5] T. Graupl, M. Ehammer, and C.-H. Rokitansky, "L-dacs 1 data link layer design and performance," in *Integrated Communications, Navigation and Surveillance Conference, 2009. ICNS'09.* IEEE, 2009, pp. 1–12.

[6] "Report itu-r m.2171," ITU, 12 2009.

[7] R. SC-228, "Rtca paper no. 075-14/pmc-1201: Command and control (c2) data link white paper," 2014.

[8] Nokia-Oyj, "Using air-to-ground lte for in-flight ultra-broadband," 2016.

[9] G. Bartoli, R. Fantacci, and D. Marabissi, "Aeromacs: A new perspective for mobile airport communications and services," *IEEE Wireless Communications*, vol. 20, no. 6, pp. 44–50, December 2013.

[10] M. Ehammer, E. Pschernig, and T. Gräupl, "Aeromacsan airport communications system," in *Digital Avionics Systems Conference (DASC), 2011 IEEE/AIAA 30th*. IEEE, 2011, pp. 4C1–1.

[11] "Report itu-r m.2205," ITU, 11 2010.

[12] "Rec. itu-r p.838-3: Specific attenuation model for rain for use in prediction methods," ITU, 2005.

[13] "Rec. itu-r p.676-11: Attenuation by atmospheric gases," ITU, 2016.

[14] U. Epple, "Ofdm receiver concept for the aeronautical communications system ldacs1 to cope with impulsive interference," Ph.D. dissertation, University of Ulm, 11 2014.

[15] P. Hoeher and E. Haas, "Aeronautical channel modeling at vhf-band," in *Gateway to 21st Century Communications Village. VTC 1999-Fall. IEEE VTS 50th Vehicular Technology Conference (Cat. No.99CH36324)*, vol. 4, 1999, pp. 1961–1966 vol.4.

[16] D. W. Matolak and R. Sun, "Air-ground channel characterization for unmanned aircraft systems - part i: Methods, measurements, and models for over-water settings," *IEEE Transactions on Vehicular Technology*, vol. 66, no. 1, pp. 26–44, Jan 2017.

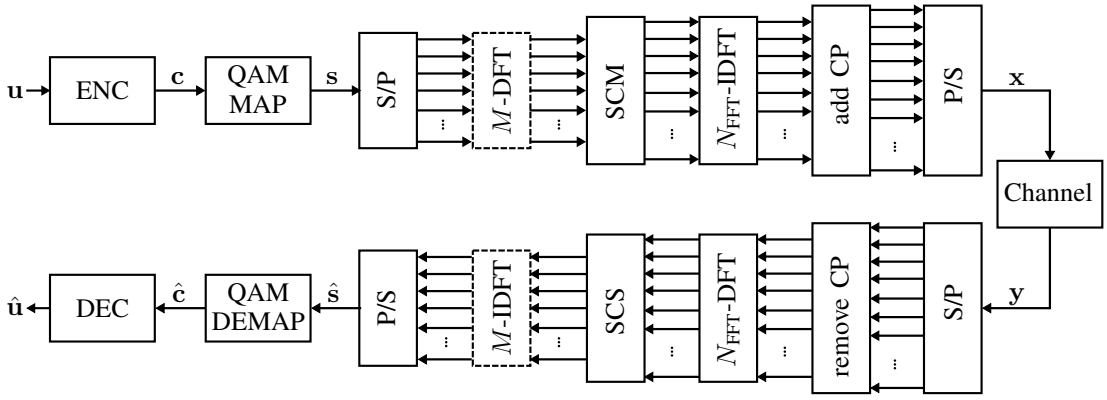

Fig. 5: Block diagram of the transmission system with focus on the OFDM and SC-FDMA structure, respectively. Dashed boxes indicate blocks that are used for SC-FDMA only. ENC/DEC denotes an encoder/decoder, S/P and P/S denotes a serial-to-parallel or parallel-to-serial converter, SCM is the subcarrier mapping, SCS the subcarrier selection, CP denotes the cyclic prefix. The Quadtrature Amplitude Modulation (QAM) modulator/demodulator can also be replaced by a Phase Shift Keying (PSK) modulator/demodulator. The (inverse) Discrete Fourier Transform ((I)DFT) can be implemented by a (inverse) Fast Fourier Transform ((I)FFT). Please note, that in a practical setup pulse shaping and radio frequency upmixing needs to be added at the transmitter and downmixing, filtering, time and frequency synchronization as well as channel estimation and signal equalization to the receiver side.

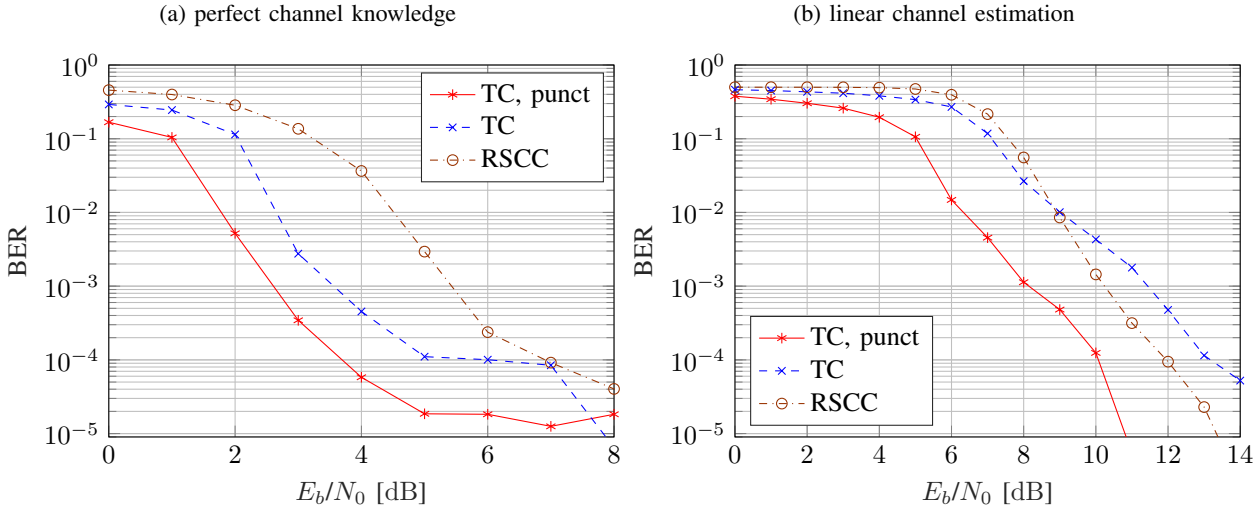

Fig. 6: Bit Error Ratio (BER) versus bit energy to noise ratio (E_b/N_0) for the TMA scenario for the SC-FDMA case. RSCC denotes the concatenated Reed-Solomon/convolutional code, TC denotes the turbo code.

[17] R. Sun and D. W. Matolak, "Air-ground channel characterization for unmanned aircraft systems - part ii: Hilly and mountainous settings," *IEEE Transactions on Vehicular Technology*, vol. 66, no. 3, pp. 1913–1925, March 2017.

[18] P. Pulini, S. Plass, L. Taponecco, M. Morelli, and L. Sanguinetti, "Aeromacs evolution - extension to landing, take-off, and approach phases," in *2013 Integrated Communications, Navigation and Surveillance Conference (ICNS)*, April 2013, pp. 1–14.

[19] E. Haas, "Aeronautical channel modeling," *IEEE Transactions on Vehicular Technology*, vol. 51, no. 2, pp. 254–264, Mar 2002.

[20] I. Sen and D. W. Matolak, "The 5-ghz airport surface area channel - part ii: Measurement and modeling results for small airports," *IEEE Transactions on Vehicular Technology*, vol. 57, no. 4, pp. 2027–2035, July 2008.

[21] S. Gligorevic and P. Pulini, "Simplified airport surface channel model based on the wssus assumption," in *2010 Integrated Communications, Navigation and Surveillance Conference Proceedings*, May 2010, pp. F2–1–F2–11.

[22] M. Sajatovic, B. Haindl, U. Epple, and T. Gräupl, "Updated ldacs1 system specification," *SESAR P15*, vol. 2, 2011.

[23] G. P. Calzolari, E. Vassallo, and S. Habinc, "Ccsds telemetry channel coding: the turbo coding option," in *IEE 5th CCSDS Workshop New Technologies, New Standards (Ref. No. 1998/519)*, Nov 1998, pp. 5/1–5/6.

[24] S. H. Han and J. H. Lee, "An overview of peak-to-average power ratio reduction techniques for multicarrier transmission," *IEEE Wireless Communications*, vol. 12, no. 2, pp. 56–65, April 2005.

[25] H. G. Myung, J. Lim, and D. J. Goodman, "Single carrier fdma for uplink wireless transmission," *IEEE Vehicular Technology Magazine*, vol. 1, no. 3, pp. 30–38, Sept 2006.

(a) ENR

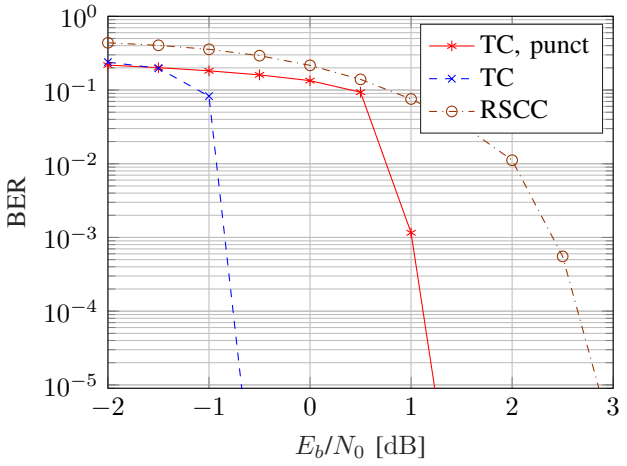

(b) TMA

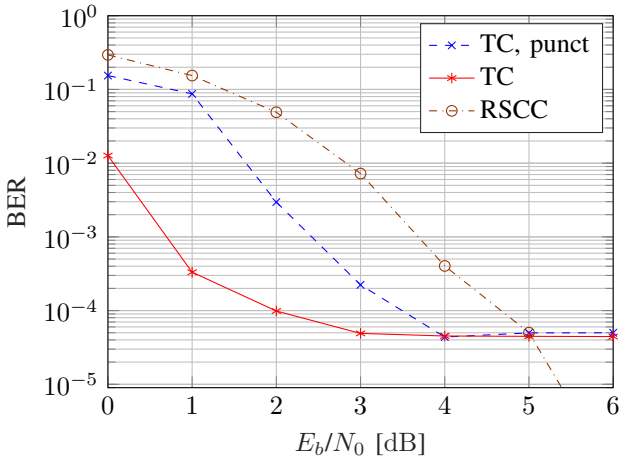

(c) APT

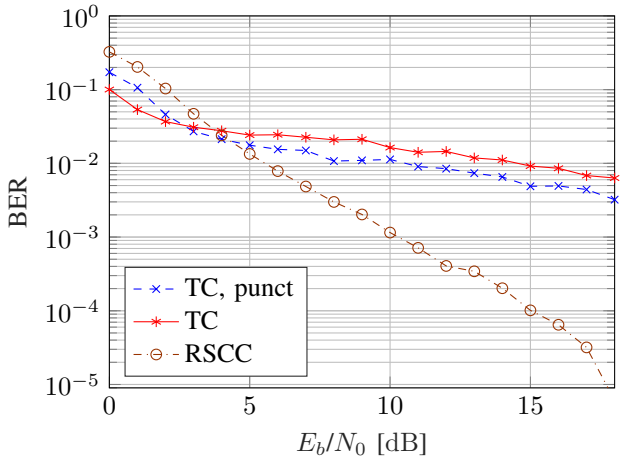

Fig. 7: Bit Error Ratio (BER) versus bit energy to noise ratio (E_b/N_0) for different scenarios for the OFDM case. RSCC denotes the concatenated Reed-Solomon/convolutional code, TC denotes the turbo code. Perfect channel knowledge is assumed.

(a) ENR

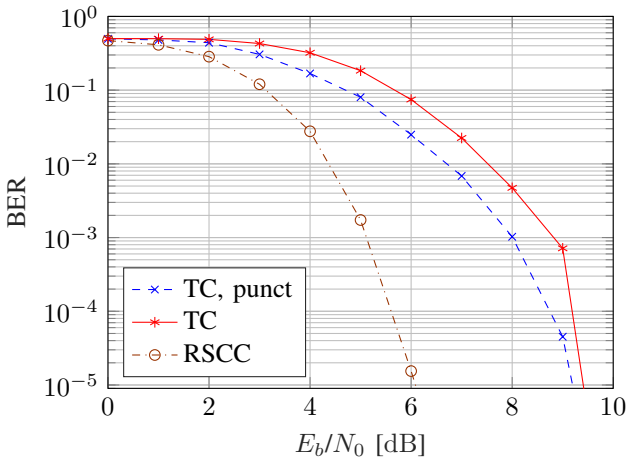

(b) TMA

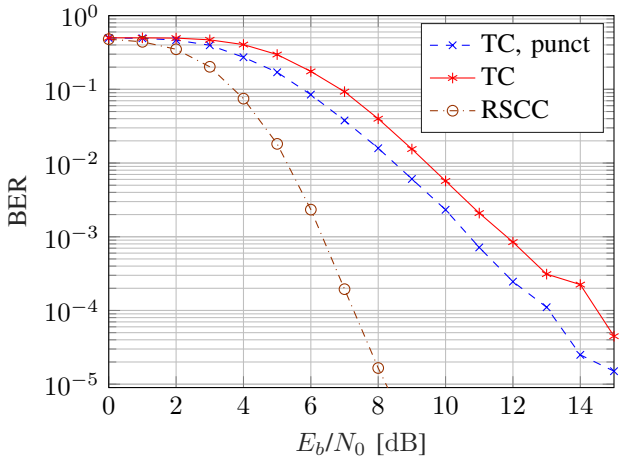

(c) APT

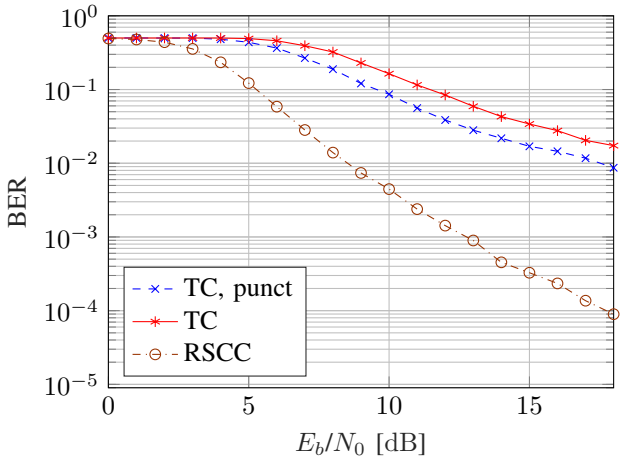

Fig. 8: Bit Error Ratio (BER) versus bit energy to noise ratio (E_b/N_0) for different scenarios for the OFDM case. RSCC denotes the concatenated Reed-Solomon/convolutional code, TC denotes the turbo code. Linear channel estimation is assumed.